

# Hybrid Video Anomaly Detection for Anomalous Scenarios in Autonomous Driving

Daniel Bogdoll\*, Jan Imhof\*, Tim Joseph, J. Marius Zöllner  
FZI Research Center for Information Technology  
KIT Karlsruhe Institute of Technology  
bogdoll@fzi.de

**Abstract:** In autonomous driving, the most challenging scenarios are the ones that can only be detected within their temporal context. Most video anomaly detection approaches focus either on surveillance or traffic accidents, which are only a sub-field of autonomous driving. In this work, we present HF<sup>2</sup>-VAD<sub>AD</sub>, a variation of the HF<sup>2</sup>-VAD surveillance video anomaly detection method for autonomous driving. We learn a representation of normality from a vehicle’s ego perspective and evaluate pixel-wise anomaly detections in rare and critical scenarios.

**Keywords:** Autonomous Driving, Anomaly Detection, Behavioral Anomalies

## 1 Introduction

In autonomous driving, the detection of anomalies is crucial for ensuring safety and reliability. Video anomaly detection (VAD) focuses on identifying events in video data that deviate from an expected normality. In autonomous driving, the challenges of detection are complicated by factors such as camera movements, ever-changing backgrounds, and rapid changes in vehicle speed.

Many different types of anomalies exist [1, 2, 3], with many approaches trying to detect them [4]. We can distinguish between five key techniques: Reconstruction, prediction, generative modeling, feature extraction, and confidence evaluation [5]. Reconstruction-based methods focus on learning a representation of normality and labeling deviations from this norm [6, 7]. Predictive approaches detect anomalies when future predictions deviate significantly from observations [8, 9]. However, in autonomous driving, most of the anomaly detection methods that are based on raw sensory data focus on atypical objects rather than atypical behaviors. Temporal anomalies are typically detected in object-based trajectory data, assuming perfect perception [10, 11, 12, 13]. The most complex temporal anomalies are *anomalous scenarios*, which pose a high risk of collision [1].

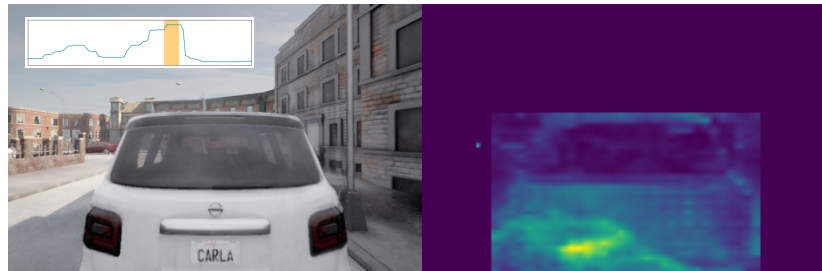


Figure 1: Exemplary anomaly detection with HF<sup>2</sup>-VAD<sub>AD</sub>. In the left frame, the vehicle in front performs a rare sudden braking maneuver in simulation, as highlighted in yellow in the top-left graph. The graph shows the anomaly scores per frame, peaking while the vehicle performs the maneuver. The right frame shows pixel-wise anomaly scores for all instances of the class *vehicle*.

\*These authors contributed equally

Table 1: Behavioral, pixel-wise anomaly detection methods for vehicle camera data in motion.

| Method                                  | Year | High Resolution | Required Sub-Methods |            |      |      |          |          |              | Anomaly Detection |                   |
|---|------|-----------------|----------------------|------------|------|------|----------|----------|--------------|-------------------|-------------------|
|   |      |                 | ROI                  | (BEV) Mask | Bbox | Flow | Odometry | Tracking | Motion Pred. |                   | Graph             |
| AnoPred [8, 54, 55]                     | 2019 | —               |                      | ×          |      |      |          |          |              |                   | Learned Normality |
| CC-Detector [53]                        | 2019 | —               | ×                    | ×          |      |      |          |          |              |                   | Learned Normality |
| SSC-TAD [56]                            | 2022 | —               |                      |            | ×    | ×    |          |          | ×            |                   | Learned Normality |
| FOL [55, 54]                            | 2023 | ✓               |                      |            | ×    | ×    | ×        |          | ×            |                   | Learned Normality |
| AnoPred <sub>Mask</sub> [8, 55]         | 2023 | —               |                      |            |      | ×    |          |          |              |                   | Learned Normality |
| AccPred [15]                            | 2023 | ✓               |                      | ×          | ×    |      |          |          |              | ×                 | Metric-based      |
| HF <sup>2</sup> -VAD <sub>AD</sub> [18] | 2024 | ✓               |                      |            | ×    | ×    |          |          |              |                   | Learned Normality |

Until recently, mostly accident-focused benchmarks were available to evaluate temporal anomalies in the context of autonomous driving [14]. Given a rise in datasets with novel dynamic anomalies [15, 16, 17], we are interested in the applicability of video anomaly detection methods for autonomous driving. Among recent state-of-the-art methods, we choose HF<sup>2</sup>-VAD as the representative model [18] and adapt it to the field of autonomous driving. For this purpose, we train a HF<sup>2</sup>-VAD<sub>AD</sub> model on simulated data representing normality and evaluate it on the challenging AnoVox dataset [17] with *anomalous scenarios* in the form of sudden braking maneuvers of the lead vehicle. We introduce a pixel-wise evaluation of HF<sup>2</sup>-VAD<sub>AD</sub> to also localize anomalies.

## 2 Related Work

There are three typical camera perspectives for anomaly detection methods in the traffic domain. *Birds-Eye-View (BEV)* and *surveillance* perspectives come from external data providers, while an ego or *dashcam* view can be provided by a vehicle itself [14]. Numerous works have focused on specific scenarios, including the detection of atypical activity in urban surveillance, the analysis of irregularities in pedestrian dynamics, and the monitoring of abnormal behavior patterns in crowds [19, 20, 21, 22, 23, 24, 25, 26, 27] as well as street scenes recorded by city cameras that evaluate vehicle behavior from an outside perspective [28, 29].

Especially the VAD subfields traffic anomaly detection [30, 31] and road accident detection [32] have gained much traction. However, only a few methods in the literature specifically analyze behavioral anomalies from the perspective of a vehicle’s onboard cameras. For our comparison in Table 1, we have also excluded frame-wise [33, 34, 35, 36] or supervised [37, 38, 39, 40] methods as well as such that focus on domain-level anomalies [41, 42, 43, 44].

In general video anomaly detection, hybrid methods that combine both reconstruction and prediction methods have emerged as the current state-of-the-art. These methods aim to utilize the strengths of both approaches by leveraging temporal dynamics and reconstruction capabilities to improve anomaly detection [45, 46, 18, 47, 48, 49]. Among these, HF<sup>2</sup>-VAD by Liu et al. [18], who built upon the work of Park et al. [50], is commonly used in the literature as a benchmark for the state of the art in video anomaly detection [51] and often serves as the foundation for further advancements [52]. It detects unusual events that deviate from normal patterns for surveillance tasks.

The idea of predicting future frames for the purpose of anomaly detection became popular around 2019, where it was demonstrated both for surveillance tasks [8] and autonomous driving [53, 54]. Liu et al. combined future frame predictions with an optical flow [8], and Bolte et al. focused on semantically distinguishing relevant classes from the rest of an image [53]. Yao et al., on the other hand, focused on predicting only the bounding boxes of relevant classes in order to compensate for the motion of the ego vehicle, which makes the prediction of whole frames more complex [54]. Later, Fang et al. built upon their work but removed the need for an odometry estimation for the ego vehicle. Recently, Yao et al. extended their own work and also provided an updated version of Liu’s approach by adding masks for relevant objects, similar to how Bolte approached the topic [55]. Finally, the new DeepAccident dataset by Wang et al. also proposed an accident detection method based on future trajectories and their distances to each other [15]. As shown in Table 1, most of the methods require many additional sub-methods to function, making them rather complex and only recently began to work for high-resolution input images.

### 3 Methodology

As shown in Section 2 and Table 1, existing video anomaly detection methods for autonomous driving are either overly complex or incapable of dealing with high-resolution input data. Based on HF<sup>2</sup>-VAD [18], our adaption HF<sup>2</sup>-VAD<sub>AD</sub> is capable of utilizing high-resolution video streams, learns a representation of normality in the domain of autonomous driving and only requires two sub-methods. Thus, it is the least complex method for video anomaly detection in the field of autonomous driving for high-resolution input.

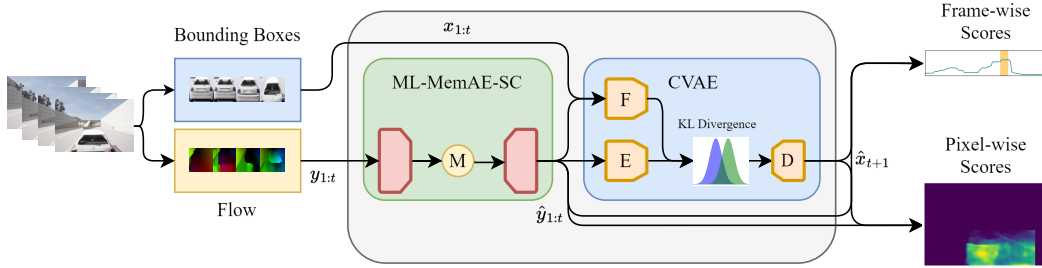


Figure 2: HF<sup>2</sup>-VAD<sub>AD</sub>: Adaptation and extension of HF<sup>2</sup>-VAD for autonomous driving. Optical flows  $y_{1:t}$  and bounding boxes  $x_{1:t}$  for relevant objects are generated for each input image. ML-MemAE-SC reconstructs the optical flows  $\hat{y}_{1:t}$  with memory-modules  $M$  to better reconstruct only normal patterns. The CVAE predicts a future frame  $\hat{x}_{t+1}$ . On this basis, image-wise and localized pixel-wise anomaly scores are generated. Adapted from [18].

**HF<sup>2</sup>-VAD.** Here, we provide a brief overview of the hybrid framework HF<sup>2</sup>-VAD [18] we build upon and refer to the original publication for further details. The framework combines Multi-Level Memory modules in an Autoencoder with Skip Connections (ML-MemAE-SC) for optical flow reconstructions and a Conditional Variational Autoencoder (CVAE) for future frame predictions. The framework is trained on normal data and uses discrepancies in the reconstructions and predictions to identify anomalies. Experiments were conducted with well-established surveillance datasets.

The *ML-MemAE-SC* uses an autoencoder structure with multiple memory modules at different levels. This structure improves the model’s ability to learn and retain typical data patterns from the training set and distinguish them from anomalies. The integration of skip connections between the encoder and decoder helps to preserve important data that might otherwise be lost during the encoding process. This part focuses on the accurate reconstruction of normal data. The training of the ML-MemAE-SC includes a composite loss function that summarizes reconstruction and entropy losses. The reconstruction loss is calculated based on the Euclidean distance.

The *CVAE* plays a central role in predicting future images by using conditioned historical data to simulate probable future scenarios. It determines the latent variable  $z_{t+1}$  by considering both the current image  $x_t$  and the optical flow  $y_{t,t+1}$  between successive images. It works on the premise that a latent variable  $z$ , representing the probabilistic state of the following image, can be derived from the immediate past to subsequently influence the generation of  $\hat{x}_{t+1}$ . It uses the encoded optical flow and the current image to estimate the posterior distribution  $p(z_{t+1}|x_t, y_{t,t+1})$ . A sample from this distribution, which represents the probabilistic state of the next image, is then drawn for image generation. During training, this latent variable  $z$  is combined with the conditions derived from the encoder  $E$  and processed by the decoder  $D$  to create the future image  $\hat{x}_{t+1}$ .

At test time, anomaly detection is performed frame-wise. The frame-wise anomaly score  $S_f$  is a fusion of the flow reconstruction error  $S_r$  and the error in the prediction of future images  $S_p$ , standardized by their respective means  $\mu$  and standard deviations  $\sigma$  from the training samples:

$$S_f = w_r \cdot \frac{S_r - \mu_r}{\sigma_r} + w_p \cdot \frac{S_p - \mu_p}{\sigma_p} \quad (1)$$

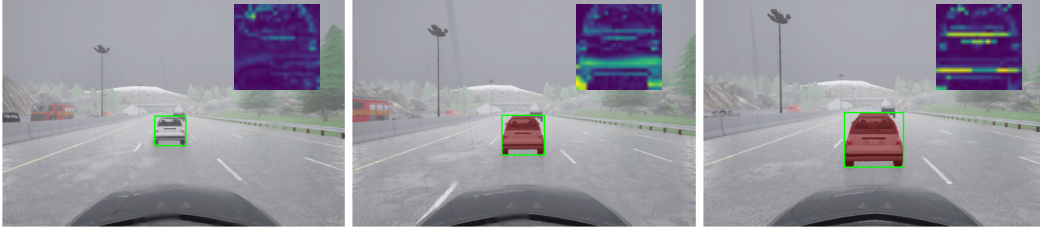


Figure 3: **Sequential Anomaly Detection:** The first image shows the normal driving mode of the lead vehicle, while the last two images show an anomaly with the pixel-wise ground truth overlaid in red.  $\text{HF}^2\text{-VAD}_{AD}$  successfully detects the unknown maneuver.

**$\text{HF}^2\text{-VAD}_{AD}$ .** First, we adapt  $\text{HF}^2\text{-VAD}$  to autonomous driving by generating dense, pixel-wise anomaly scores for the whole frame rather than focusing on the content of unlocalized, detected bounding boxes alone, as can be seen in Figure 1. We learn flow reconstructions and flow-guided frame prediction from the perspective of an ego-vehicle rather than from the perspective of a static surveillance camera. Our training dataset was collected with the CARLA simulation engine [57]. Rather than collecting data with the default autopilot, we employ Roach [58] as the driving agent.

To reflect the complexity of real-world traffic, the training dataset features four different cities, each with its own weather and traffic dynamics. The training data includes 38 scenarios with over 30,000 high-resolution frames with a resolution of 600 x 800 pixels. Crucially, the training dataset contains only normal driving scenes so that the model can internalize a baseline of normal traffic behavior, which is crucial for detecting deviations that indicate anomalies in real-world driving situations. Other normally behaving agents, including lead vehicles, are included in the training data.

Flows are generated by FlowNet2.0 [59] to ensure that both static and motion-based features contribute to the training of the model. Bounding boxes are detected with an off-the-shelf object detection model [60] trained on CARLA data.

We first train the ML-MemAE-SC with the extracted flows from the training dataset, then train the CVAE model with the reconstructed flows from the ML-MemAE-SC and the corresponding frames, and finally fine-tune the whole framework. During fine-tuning, the weights of the two models are adjusted together to improve their coordination and the overall accuracy of anomaly detection.

We train the model specifically on foreground objects, i.e., *vehicles*, extracted from these images with bounding boxes, and construct spatiotemporal cubes (STC) for each object, where the dimensions of these cubes are standardized to 32x32. The use of bounding boxes for each vehicle in the scene allows the model to focus specifically on regions within the image where temporal anomalies in the form of unexpected maneuvers can occur.

In addition to the existing frame-wise anomaly detection, we have integrated a pixel-wise anomaly detection. For this, the anomaly score for each pixel, denoted by  $S_{\text{pixel}}$ , is derived from a weighted average of robustly scaled mean squared errors (MSE) for optical flow and image prediction:

$$S_{\text{pixel}} = w_{r,p} \cdot m_r + w_{p,p} \cdot m_p \quad (2)$$

The variables  $m_r$  and  $m_p$  denote the mean values of the robustly scaled MSEs for the optical flow and image prediction, respectively. The scores are calculated using the weights  $w_{r,p}$  for optical flow and  $w_{p,p}$  for image prediction. Robust scaling is used to standardize the MSEs by reducing the influence of outliers, making the method more reliable for detecting anomalies under different conditions. The averaging process calculates the mean of these scaled values to summarize the error across all pixels. The resulting pixel-wise scores are then used to localize anomalies within the image. A score of 0 is set for all pixels outside the bounding boxes, as shown in Figure 1. In contrast, the frame-wise approach of the original  $\text{HF}^2\text{-VAD}$  uses simple summation and normalization based on the training statistics. Specifically, the sum of MSE losses across all dimensions is calculated for

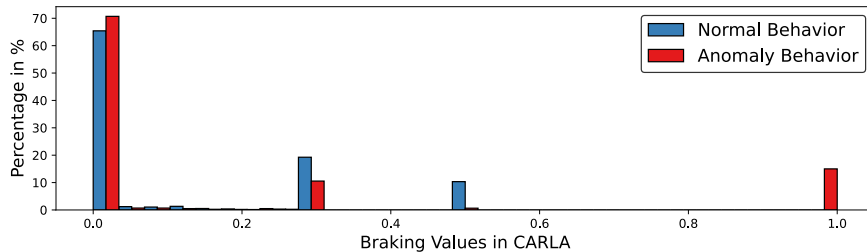


Figure 4: Distribution of braking behavior in training (blue) and test (red) data. High-intensity sudden braking scenarios only occur in the evaluation dataset.

both optical flow and image predictions, and these summed values are then normalized using the mean and standard deviation from the training data. In the presence of detections, they add up all  $32 \times 32$  anomaly patches and choose the largest value as the frame-wise anomaly score. We also report these frame-wise results as  $\text{AUROC}^\circ$  in Section 4.

In contrast, our approach calculates a pixel-wise anomaly score by normalizing and aggregating mean-squared errors of optical flow and frame predictions, then scaling these scores to bounding boxes within each frame. This pixel-wise approach allows for a more granular analysis, focusing on specific areas within frames rather than a single aggregated frame-level score.

## 4 Evaluation

For the evaluation, we used the recently released AnoVox benchmark [17] with *anomalous scenarios* in the form of sudden braking maneuvers performed by lead vehicles, as visible in Figure 3. These are common and dangerous situations in road traffic [61] and are not included in our training data, as Figure 4 shows. In the 13 evaluation scenarios, the ego-vehicle follows a lead vehicle along a longer route under different weather and traffic conditions. At certain intervals, the lead vehicle performs a sudden braking maneuver. We extended the available pixel-wise ground truth, as shown in Figure 3 by frame-wise annotations. The annotation of the anomalies started with the unexpected sudden braking of the leading vehicle and ended with its complete stop.

Table 2: Evaluation and ablation studies of  $\text{HF}^2\text{-VAD}_{AD}$  and  $\text{ML-MemAE-SC}$  under different scenarios, with **best** and second-best results highlighted.

| Model                               | Domain  | Weather  | Finetuned | $\text{AUROC}^\circ \uparrow$ | $\text{FPR}_{95} \downarrow$ | $\text{IoU} \uparrow$ |
|-------------------------------------|---------|----------|-----------|-------------------------------|------------------------------|-----------------------|
| <i>Bounding Boxes: Detection</i>    |         |          |           |                               |                              |                       |
| $\text{HF}^2\text{-VAD}_{AD}$       | All     | All      | ✓         | 66.98                         | <b>2.58</b>                  | 48.10                 |
| $\text{HF}^2\text{-VAD}_{AD}$       | City    | Sunshine | ✓         | 68.04                         | 2.48                         | 48.09                 |
| $\text{HF}^2\text{-VAD}_{AD}$       | City    | Rain     | ✓         | <u>69.74</u>                  | <u>2.68</u>                  | <u>51.30</u>          |
| $\text{HF}^2\text{-VAD}_{AD}$       | Highway | Sunshine | ✓         | 57.22                         | 3.15                         | <b>60.71</b>          |
| $\text{HF}^2\text{-VAD}_{AD}$       | Highway | Rain     | ✓         | <b>76.60</b>                  | <b>1.34</b>                  | 41.09                 |
| <i>Bounding Boxes: Ground Truth</i> |         |          |           |                               |                              |                       |
| $\text{ML-MemAE-SC}$                | All     | All      | —         | 67.49                         | 7.80                         | —                     |
| $\text{HF}^2\text{-VAD}_{AD}$       | All     | All      | —         | <u>81.01</u>                  | 3.72                         | —                     |
| $\text{HF}^2\text{-VAD}_{AD}$       | All     | All      | ✓         | 79.09                         | <b>2.83</b>                  | —                     |
| $\text{HF}^2\text{-VAD}_{AD}$       | City    | Sunshine | ✓         | 80.74                         | 3.10                         | —                     |
| $\text{HF}^2\text{-VAD}_{AD}$       | City    | Rain     | ✓         | 74.08                         | <u>3.05</u>                  | —                     |
| $\text{HF}^2\text{-VAD}_{AD}$       | Highway | Sunshine | ✓         | 74.76                         | 3.19                         | —                     |
| $\text{HF}^2\text{-VAD}_{AD}$       | Highway | Rain     | ✓         | <b>91.74</b>                  | 99.32                        | —                     |

In order to evaluate the performance of  $\text{HF}^2\text{-VAD}_{AD}$ , we provide both quantitative and qualitative insights. Two metrics are used for evaluation: the already used Area Under the Receiver Operation Characteristic ( $\text{AUROC}^\circ$ ) for frame-wise evaluations and the False Positive Rate at 95% True Positive Rate ( $\text{FPR}_{95}$ ) for pixel-wise evaluation. The AUROC metric, widely used in the

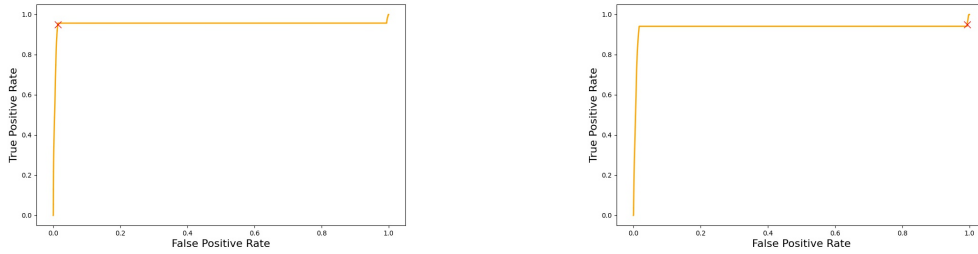


Figure 5: Comparison of ROC curves for the setting *highway with rain*. The x marks the  $FPR_{95}$  position. On the left, a low  $FPR_{95}$  is achieved with predicted bounding boxes. On the right, the  $FPR_{95}$  rose sharply with ground truth bounding boxes.

VAD literature [62, 18, 63, 64], serves as a measure of VAD accuracy by varying the threshold for anomaly assessment, with higher AUROC values indicating better detection performance. Adding  $FPR_{95}$  [65, 66] provides insights into the false-positive rates if nearly all anomalies are correctly detected, with lower values indicating better detection performance. Since our detected bounding boxes do not fully match the existing ground truth, we only evaluate the  $FPR_{95}$  based on the overlapping area and also provide the IoU to demonstrate the quality of the bounding boxes.

#### 4.1 Quantitative Results

As shown in Table 2, we perform various experiments to better understand the performance of  $HF^2-VAD_{AD}$  under varying conditions. Comparing city and highway scenarios, we observe a strong sensitivity of the model to these environments, but no clear trend emerges. For highway settings with bad weather, we can observe poor performance. As the pixel-wise anomaly scores are only calculated for bounding boxes and all other pixels are set to 0, there is generally a low false positive rate. However, if more than 5% of the ground truth anomalies are not detected, detecting all anomalous pixels requires a threshold close to zero. This results in the entire image being detected as anomalous, causing the  $FPR_{95}$  to rise sharply, as shown in Figure 5.

Table 3: Empirical study to determine the effects of different weights for  $HF^2-VAD_{AD}$ .

| $w_r$ and $w_{r_p}$ | $w_p$ and $w_{p_p}$ | $FPR_{95} \downarrow$ | $AUROC^\diamond \uparrow$ |
|---------------------|---------------------|-----------------------|---------------------------|
| 10                  | 0.1                 | <b>2.83</b>           | <u>79.09</u>              |
| 1                   | 0.1                 | <u>2.86</u>           | 78.78                     |
| 1                   | 0                   | <b>2.83</b>           | <b>79.13</b>              |
| 0                   | 1                   | 96.67                 | 69.15                     |
| 0.1                 | 1                   | 4.05                  | 76.20                     |
| 0.1                 | 10                  | 95.78                 | 70.70                     |

To determine optimal values for the weights, as introduced in Section 3, we performed an empirical study, as shown in Table 3. While we observe the best results in the case when we completely neglect image predictions, we decided to set  $w_r, w_{r_p} = 10$  and  $w_p, w_{p_p} = 0.1$ , as the performance metrics were too small to be significant, and we wanted to retain the advantages of both modules. The study showed that the model performs significantly worse when image prediction is weighted higher, which is in contrast to the original implementation of  $HF^2-VAD$ , in which the frame prediction was weighted higher than the flow reconstruction, with the weight for frame prediction set to 1 and the weight for flow reconstruction set to 0.1.

**Ablation Studies.** To better understand the performance of our approach, we perform three types of ablation studies. First, we only utilize the intermediate outputs of the ML-ML-MemAE-SC to evaluate isolated flow reconstructions.

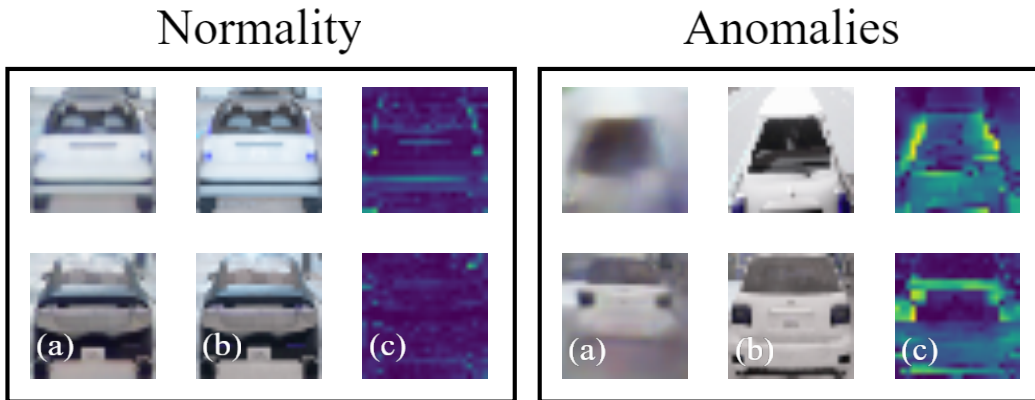


Figure 6: On the left, two normal scenarios are shown. Here, the model’s next-frame predictions (a) match the actual next frames (b) closely. On the right, we have shown sudden brake scenarios. Here, significant prediction differences arise, leading to high pixel-wise anomaly values (c).

Second, we evaluate both bounding boxes generated from an off-the-shelf object detection model [60] and ground truth bounding boxes from the evaluation dataset to isolate the effect of model failures. We can observe that bounding boxes are best detected in simpler highway settings with good weather. The IoU performance suffers especially from poor detections of distant objects. Since mostly irrelevant vehicle are missing in the detections, we see improved  $FPR_{95}$  values for bounding box detections, but at the cost of reduced AUROC scores.

Lastly, we examine the influence of the fine-tuning stage during training. After fine-tuning,  $HF^2-VAD_{AD}$  shows an improvement in precision. While the AUROC decreases slightly, the model achieves a better balance in the performance metrics with a significantly lower  $FPR_{95}$ .

## 4.2 Qualitative Results

In Figure 6, we show a series of comparative visualizations demonstrating the performance of  $HF^2-VAD_{AD}$  in traffic scenarios. The model is able to predict regular behaviors very well, while atypical ones lead to poor predictions and, thus, high anomaly scores. The pixel-wise anomaly maps serve as a meaningful indicator, with more highlighted areas signaling larger prediction discrepancies. For normal driving patterns, these maps show only small deviations from ground truth, indicating that the model can predict the subsequent images well. For anomalies, the model often predicts, as it learned, that the vehicle maintains the distance. This leads to positive anomaly detections, as the vehicle is currently anomalous and getting closer due to the braking maneuver. This can be recognized by the increased highlighting in the difference maps.

**Failure Cases.** As shown in Figure 7, there are certain cases which are challenging. The first image shows how the model often incorrectly produces high anomaly scores when a lead vehicle is turning rather than going straight. The middle image shows a scene where the object detection model has problems with detecting objects in unfavorable weather conditions, such as heavy rain so anomaly detection is not possible.

## 5 Conclusion

In summary, our research has shown that  $HF^2-VAD$ , a framework originally developed for detecting anomalies in surveillance systems can be effectively transferred to the field of autonomous driving. By extending it to dense pixel-wise anomaly maps and creating a dedicated training and test dataset, we have validated the effectiveness of  $HF^2-VAD_{AD}$  in the vehicle context, bridging the gap between static monitoring and dynamic vehicle environments.



Figure 7: **Failure Cases:** The model can produce high pixel-wise anomaly scores for turning vehicles, as shown on the left. Here, the encircled area in the frame-wise graph shows the duration of the curve. In the middle, a missing bounding box detection during bad weather situations leads to no anomaly detection at all. On the right, the bounding box only captures a part of the lead vehicle, and a truck in the back is completely missed.

Our contributions further include the extension to dense anomaly detections, domain-specific weight adaptations, and dealing with multiple bounding boxes separately rather than combining them into one score, using robust scaling. In the future, we aim to further refine the framework to better deal with the known failure cases and evaluate more types of anomalies to examine its performance among a wider variety of scenarios, such as wrong-way drivers.

## References

- [1] J. Breitenstein, J.-A. Termöhlen, D. Lipinski, and T. Fingscheidt. Systematization of corner cases for visual perception in automated driving. In *IEEE Intelligent Vehicles Symposium (IV)*, 2020. 1
- [2] F. Heidecker, J. Breitenstein, K. Rösch, J. Löhdefink, M. Bieshaar, C. Stiller, T. Fingscheidt, and B. Sick. An application-driven conceptualization of corner cases for perception in highly automated driving. In *IEEE Intelligent Vehicles Symposium (IV)*, 2021. 1
- [3] D. Bogdoll, J. Breitenstein, F. Heidecker, M. Bieshaar, B. Sick, T. Fingscheidt, and J. M. Zollner. Description of corner cases in automated driving: Goals and challenges. In *IEEE/CVF International Conference on Computer Vision Workshops (ICCVW)*, 2021. 1
- [4] D. Bogdoll, M. Nitsche, and J. M. Zöllner. Anomaly Detection in Autonomous Driving: A Survey. In *2022 IEEE/CVF Conference on Computer Vision and Pattern Recognition Workshops (CVPRW)*, pages 4487–4498, 2022. 1
- [5] J. Breitenstein, J.-A. Termöhlen, D. Lipinski, and T. Fingscheidt. Corner cases for visual perception in automated driving: Some guidance on detection approaches. *arXiv:2102.05897*, 2021. 1
- [6] M. Hasan, J. Choi, J. Neumann, A. K. Roy-Chowdhury, and L. S. Davis. Learning Temporal Regularity in Video Sequences, 2016. 1
- [7] W. Luo, W. Liu, and S. Gao. Remembering history with convolutional LSTM for anomaly detection. *2017 IEEE International Conference on Multimedia and Expo (ICME)*, pages 439–444, 2017. 1
- [8] W. Liu, W. Luo, D. Lian, and S. Gao. Future Frame Prediction for Anomaly Detection - A New Baseline. In *2018 IEEE/CVF Conference on Computer Vision and Pattern Recognition*, pages 6536–6545, 2018. 1, 2
- [9] G. Yu, S. Wang, Z. Cai, E. Zhu, C. Xu, J. Yin, and M. Kloft. Cloze Test Helps: Effective Video Anomaly Detection via Learning to Complete Video Events. In *Proceedings of the 28th ACM International Conference on Multimedia*, pages 583–591, 2020. 1



- [10] J. Wiederer, A. Bouazizi, M. Troina, U. Kressel, and V. Belagiannis. Anomaly detection in multi-agent trajectories for automated driving. In *Conference on Robot Learning*, 2021. 1
- [11] R. Jiao, J. Bai, X. Liu, T. Sato, X. Yuan, Q. A. Chen, and Q. Zhu. Learning representation for anomaly detection of vehicle trajectories. *arXiv:2303.05000*, 2023. 1
- [12] A. Breuer, Q. Le Xuan, J.-A. Termöhlen, S. Homoceanu, and T. Fingscheidt. Quo Vadis? Meaningful Multiple Trajectory Hypotheses Prediction in Autonomous Driving. In *2021 IEEE International Intelligent Transportation Systems Conference (ITSC)*, pages 637–644, 2021. 1
- [13] A. V. R. Group. Interpretable Trajectory Prediction for Autonomous Vehicles via Counterfactual Responsibility, 2023. 1
- [14] J. Fang, J. Qiao, J. Xue, and Z. Li. Vision-Based Traffic Accident Detection and Anticipation: A Survey. *IEEE Transactions on Circuits and Systems for Video Technology*, 34(4), 2024. 2
- [15] T. Wang, S. Kim, W. Ji, E. Xie, C. Ge, J. Chen, Z. Li, and P. Luo. DeepAccident: A Motion and Accident Prediction Benchmark for V2X Autonomous Driving, 2023. 2
- [16] L. Gong, Y. Zhang, Y. Xia, Y. Zhang, and J. Ji. SDAC: A Multimodal Synthetic Dataset for Anomaly and Corner Case Detection in Autonomous Driving. *Proceedings of the AAAI Conference on Artificial Intelligence*, 38(3):1914–1922, 2024. 2
- [17] D. Bogdoll, I. Hamdard, L. N. Rößler, F. Geisler, M. Bayram, F. Wang, J. Imhof, M. de Campos, A. Tabarov, Y. Yang, H. Gottschalk, and J. M. Zöllner. AnoVox: A Benchmark for Multimodal Anomaly Detection in Autonomous Driving. 2, 5
- [18] Z. Liu, Y. Nie, C. Long, Q. Zhang, and G. Li. A Hybrid Video Anomaly Detection Framework via Memory-Augmented Flow Reconstruction and Flow-Guided Frame Prediction, 2021. 2, 3, 6
- [19] V. Chandola, A. Banerjee, and V. Kumar. Anomaly detection: A survey. *ACM Computing Surveys*, 41(3):1–58, 2009. 2
- [20] O. P. Popoola and Kejun Wang. Video-Based Abnormal Human Behavior Recognition—A Review. *IEEE Transactions on Systems, Man, and Cybernetics, Part C (Applications and Reviews)*, 42(6):865–878, 2012. 2
- [21] R. Nayak, U. C. Pati, and S. K. Das. A comprehensive review on deep learning-based methods for video anomaly detection. *Image and Vision Computing*, 106:104078, 2021. 2
- [22] B. Ramachandra, M. J. Jones, and R. R. Vatsavai. A Survey of Single-Scene Video Anomaly Detection, 2020. 2
- [23] T. M. Tran, T. N. Vu, N. D. Vo, T. V. Nguyen, and K. Nguyen. Anomaly Analysis in Images and Videos: A Comprehensive Review. *ACM Computing Surveys*, 55(7):148:1–148:37, 2022. 2
- [24] K. K. Santhosh, D. P. Dogra, and P. P. Roy. Anomaly Detection in Road Traffic Using Visual Surveillance: A Survey. *ACM Computing Surveys*, 53(6):119:1–119:26, 2020. 2
- [25] A. Aldayri and W. Albattah. Taxonomy of Anomaly Detection Techniques in Crowd Scenes. *Sensors*, 22(16):6080, 2022. 2
- [26] N. Patil and P. K. Biswas. A survey of video datasets for anomaly detection in automated surveillance. In *2016 Sixth International Symposium on Embedded Computing and System Design (ISED)*, pages 43–48, Patna, India, 2016. ISBN 9781509025411. 2
- [27] S. Chandrakala, K. Deepak, and G. Revathy. Anomaly detection in surveillance videos: a thematic taxonomy of deep models, review and performance analysis. *Artificial Intelligence Review*, 56(4):3319–3368, 2023. 2

- [28] S. K. Kumaran, D. P. Dogra, and P. P. Roy. Anomaly Detection in Road Traffic Using Visual Surveillance: A Survey. *ACM Computing Surveys*, 53(6):1–26, 2021. 2
- [29] Y. Djenouri, A. Belhadi, J. C.-W. Lin, D. Djenouri, and A. Cano. A Survey on Urban Traffic Anomalies Detection Algorithms. *IEEE Access*, 7:12192–12205, 2019. 2
- [30] R. Liang, Y. Li, J. Zhou, and X. Li. Text-driven traffic anomaly detection with temporal high-frequency modeling in driving videos. *IEEE Transactions on Circuits and Systems for Video Technology*, 2024. 2
- [31] Y. Zhao, W. Wu, Y. He, Y. Li, X. Tan, and S. Chen. Good Practices and a Strong Baseline for Traffic Anomaly Detection. In *CVPR-W*, 2021. 2
- [32] J. Fang, L.-l. Li, J. Zhou, J. Xiao, H. Yu, C. Lv, J. Xue, and T.-S. Chua. Abductive Ego-View Accident Video Understanding for Safe Driving Perception. *arXiv:2403.00436*, 2024. 2
- [33] Z. Zhou, X. Dong, Z. Li, K. Yu, C. Ding, and Y. Yang. Spatio-Temporal Feature Encoding for Traffic Accident Detection in VANET Environment. *IEEE Transactions on Intelligent Transportation Systems*, 23(10), 2022. 2
- [34] S. Haresh, S. Kumar, M. Z. Zia, and Q.-H. Tran. Towards Anomaly Detection in Dashcam Videos. In *IEEE Intelligent Vehicles Symposium (IV)*, 2020. 2
- [35] S. Lagraa, M. Cailac, S. Rivera, F. Beck, and R. State. Real-Time Attack Detection on Robot Cameras: A Self-Driving Car Application. In *IEEE International Conference on Robotic Computing (IRC)*, 2019. 2
- [36] G. Aivatoglou, N. Oikonomou, G. Spanos, K. Livitckaia, K. Votis, and D. Tzovaras. EVENT: Real-time Video Feed Anomaly Detection for Enhanced Security in Autonomous Vehicles. In *Mediterranean Conference on Control and Automation (MED)*, 2023. 2
- [37] F.-H. Chan, Y.-T. Chen, Y. Xiang, and M. Sun. Anticipating Accidents in Dashcam Videos. In S.-H. Lai, V. Lepetit, K. Nishino, and Y. Sato, editors, *ACCV*, 2017. 2
- [38] H. Kim, K. Lee, G. Hwang, and C. Suh. Crash to Not Crash: Learn to Identify Dangerous Vehicles Using a Simulator. *Proceedings of the AAAI Conference on Artificial Intelligence*, 33(01), 2019. 2
- [39] T.-N. Le, S. Ono, A. Sugimoto, and H. Kawasaki. Attention R-CNN for Accident Detection. In *IEEE Intelligent Vehicles Symposium (IV)*, 2020. 2
- [40] F. Hajri and H. Fradi. Vision Transformers for Road Accident Detection from Dashboard Cameras. In *IEEE International Conference on Advanced Video and Signal Based Surveillance (AVSS)*, 2022. 2
- [41] A. Stocco, M. Weiss, M. Calzana, and P. Tonella. Misbehaviour Prediction for Autonomous Driving Systems. In *IEEE/ACM International Conference on Software Engineering (ICSE)*, 2020. 2
- [42] M. Hussain, N. Ali, and J.-E. Hong. DeepGuard: A framework for safeguarding autonomous driving systems from inconsistent behaviour. *Automated Software Engineering*, 29(1), 2021. 2
- [43] R. Grewal, P. Tonella, and A. Stocco. Predicting Safety Misbehaviours in Autonomous Driving Systems using Uncertainty Quantification. *arXiv:2404.18573*, 2024. 2
- [44] S. Bai, C. Han, and S. An. Recognizing Anomalies in Urban Road Scenes Through Analysing Single Images Captured by Cameras on Vehicles. *Sensing and Imaging*, 19(1):34, 2018. 2
- [45] M. Ye, X. Peng, W. Gan, W. Wu, and Y. Qiao. AnoPCN: Video Anomaly Detection via Deep Predictive Coding Network. *Proceedings of the 27th ACM International Conference on Multimedia*, pages 1805–1813, 2019. 2

- [46] Y. Tang, L. Zhao, S. Zhang, C. Gong, G. Li, and J. Yang. Integrating prediction and reconstruction for anomaly detection. *Pattern Recognition Letters*, 129:123–130, 2020. 2
- [47] T. Liu, C. Zhang, X. Niu, and L. Wang. Spatio-temporal prediction and reconstruction network for video anomaly detection. *PLOS ONE*, 17(5):e0265564, 2022. 2
- [48] Q. Li, R. Yang, Y. Shen, and Z. Zhang. Dual-Branch Framework with Convolutional Attentive Block for Video Anomaly Detection, 2022. 2
- [49] H. Huang, B. Zhao, F. Gao, P. Chen, J. Wang, and A. Hussain. A Novel Unsupervised Video Anomaly Detection Framework Based on Optical Flow Reconstruction and Erased Frame Prediction. *Sensors*, 23(10):4828, 2023. 2
- [50] H. Park, J. Noh, and B. Ham. Learning Memory-Guided Normality for Anomaly Detection. In *IEEE/CVF Conference on Computer Vision and Pattern Recognition (CVPR)*, 2020. 2
- [51] N.-C. Ristea, F.-A. Croitoru, R. T. Ionescu, M. Popescu, F. S. Khan, and M. Shah. Self-Distilled Masked Auto-Encoders are Efficient Video Anomaly Detectors. 2023. 2
- [52] W. Wan, W. Zhang, and C. Jin. Pose-Motion Video Anomaly Detection via Memory-Augmented Reconstruction and Conditional Variational Prediction. *2023 IEEE International Conference on Multimedia and Expo (ICME)*, pages 2729–2734, 2023. 2
- [53] J.-A. Bolte, A. Bar, D. Lipinski, and T. Fingscheidt. Towards corner case detection for autonomous driving. In *IEEE Intelligent Vehicles Symposium (IV)*, 2019. 2
- [54] Y. Yao, M. Xu, Y. Wang, D. J. Crandall, and E. M. Atkins. Unsupervised Traffic Accident Detection in First-Person Videos. In *IEEE/RSJ International Conference on Intelligent Robots and Systems (IROS)*, 2019. 2
- [55] Y. Yao, X. Wang, M. Xu, Z. Pu, Y. Wang, E. Atkins, and D. J. Crandall. DoTA: Unsupervised Detection of Traffic Anomaly in Driving Videos. *IEEE Transactions on Pattern Analysis and Machine Intelligence*, 45(1), 2023. 2
- [56] J. Fang, J. Qiao, J. Bai, H. Yu, and J. Xue. Traffic Accident Detection via Self-Supervised Consistency Learning in Driving Scenarios. *IEEE Transactions on Intelligent Transportation Systems*, 23(7), 2022. 2
- [57] A. Dosovitskiy, G. Ros, F. Codevilla, A. Lopez, and V. Koltun. CARLA: An Open Urban Driving Simulator, 2017. 4
- [58] Z. Zhang, A. Liniger, D. Dai, F. Yu, and L. Van Gool. End-to-End Urban Driving by Imitating a Reinforcement Learning Coach, 2021. 4
- [59] E. Ilg, N. Mayer, T. Saikia, M. Keuper, A. Dosovitskiy, and T. Brox. FlowNet 2.0: Evolution of Optical Flow Estimation with Deep Networks, 2016. 4
- [60] MinyiLin. Carla computer vision project. *Roboflow Universe*, 2022. URL <https://universe.roboflow.com/minyilin-3nzak/carla-f4116>. visited on 2024-06-07. 4, 7
- [61] H. Kim, K. Lee, G. Hwang, and C. Suh. Crash to Not Crash: Learn to Identify Dangerous Vehicles Using a Simulator. *Proceedings of the AAAI Conference on Artificial Intelligence*, 33(01):978–985, 2019. 5
- [62] D. Gong, L. Liu, V. Le, B. Saha, M. R. Mansour, S. Venkatesh, and A. v. d. Hengel. Memorizing Normality to Detect Anomaly: Memory-augmented Deep Autoencoder for Unsupervised Anomaly Detection, 2019. 6
- [63] C. Lu, J. Shi, and J. Jia. Abnormal Event Detection at 150 FPS in MATLAB. In *2013 IEEE International Conference on Computer Vision*, pages 2720–2727, 2013. 6

- [64] V. Mahadevan, W. Li, V. Bhalodia, and N. Vasconcelos. Anomaly detection in crowded scenes. In *2010 IEEE Computer Society Conference on Computer Vision and Pattern Recognition*, pages 1975–1981, 2010. 6
- [65] J. Henriksson, C. Berger, M. Borg, L. Tornberg, S. R. Sathyamoorthy, and C. Englund. Performance Analysis of Out-of-Distribution Detection on Trained Neural Networks. *Information and Software Technology*, 130:106409, 2021. 6
- [66] G. Di Biase, H. Blum, R. Siegwart, and C. Cadena. Pixel-wise Anomaly Detection in Complex Driving Scenes, 2021. 6